ISSN 1027-4510, Journal of Surface Investigation. X-ray, Synchrotron and Neutron Techniques, 2013, Vol. 7, No. 3, pp. 401–406. © Pleiades Publishing, Ltd., 2013.
Original Russian Text © E.V. Velichko, Yu.O. Chetverikov, L.A. Aksel'rod, V.N. Zabenkin, V.V. Piyadov, A.A. Sumbatyan, W.H. Kraan, S.V. Grigor'ev, 2013, published in Poverkhnost'. Rentgenovskie, Sinkhrotronnye i Neitronnye Issledovaniya, 2013, No. 5, pp. 3–9.

Spin-Echo Small-Angle Neutron Scattering Device: Test Experiment Using SiO_2 Colloidal Particles

E. V. Velichko[a], Yu. O. Chetverikov[a], L. A. Aksel'rod[a], V. N. Zabenkin[a], V. V. Piyadov[a], A. A. Sumbatyan[a], W. H. Kraan[b], and S. V. Grigor'ev[a]

[a] *St. Petersburg Institute of Nuclear Physics, Russian Academy of Sciences, Gatchina, St. Petersburg, Russia*
[b] *Faculty of Applied Sciences, Delft University of Technology, Delft, The Netherlands*
e-mail: evgen@pnpi.spb.ru

Received April 12, 2012

Abstract—The results of the first experiments with a spin-echo small-angle neutron scattering (SESANS) device built at the VVR-M reactor at the St. Petersburg Institute of Nuclear Physics (Gatchina) are presented. SESANS utilizes the possibilities of the spin-echo method for determining the structural characteristics of materials in real space with on the $10–10^4$-nm length scale. Validation measurements are conducted using SiO_2 colloidal particles. Samples of SiO_2 spheres with a diameter determined through scanning electron microscopy and synchrotron-radiation ultra-small-angle scattering are used for calibration of the device. Approximation of the data obtained with the SESANS device was conducted using the autocorrelation function for dilute monodisperse spheres. The sizes of the spheres determined via SESANS are in agreement with those determined by other methods within the experimental error.

DOI: 10.1134/S1027451013030154

INTRODUCTION

The neutron spin-echo (NSE) method, first suggested by F. Mezei in 1972 [1, 2], is an effective method for investigating the dynamics of condensed media with the help of neutron scattering. The neutron velocity before and after scattering in the inelastic NSE is measured by the Larmor precession of the neutron spin. The scattering event in the NSE becomes obvious from the change in the Larmor precession of the neutron in magnetic fields before and after the sample. For this purpose two identical precession regions before (the first arm of the device) and after (the second arm of the device) the sample are included in the NSE device. The magnetic field in these regions is oppositely directed. Hence, the polarization of the neutron beam rotates in the two arms of the device like the hands of a clock but in different directions. After the neutron beam passes through the first arm, the "clock hand" indicates the time of passage. The second arm rotates the "clock hand" in the opposite direction and fully compensates the first arm in the case when there is no scattering. In the case of inelastic scattering on the sample, the velocities of neutron-beam passage through the first and second arms of the device are different. The difference in the time of neutron-beam passage through the first and second shoulder of the device occurs due to a difference in the velocities, which is expressed as a phase of the Larmor precession of the neutron-beam polarization. Information on the velocities of the passage through the first and second arm of the device obtained from the phase of the Larmor precession refers to the same neutron. Hence, a change in the neutron velocity in the NSE can be measured directly in one step, which is the conceptual novelty of the method. This process is in contrast to the classical approach for the measurement of inelastic scattering, in which a change in the neutron velocity is recorded with selective measuring equipment: a narrow range of initial velocities is selected before the scattering event, while after scattering only neutrons with a certain velocity and, respectively, corresponding to a certain velocity change are recorded in the scattered beam.

In 1996, T. Rekveldt suggested [3] that the NSE method be used for small-angle neutron scattering (SANS). Considering that for effective NSE implementation a noticeable difference in the time of the scattered and unscattered part of the neutron beam in the magnetic field is required (and the neutron velocities before and after the event remain equal upon elastic scattering) it was necessary to enhance the manifestation of the difference in the path lengths of the scattered and unscattered neutrons. This problem was solved by developing a "slanted geometrical shape" of the fields in both arms of the device: an acute angle is preset between the neutron beam and the plane-parallel boundaries of the magnetic field, through which the beam passes and, subsequently, the phase of the Larmor precession strongly depends on the angle where the neutron momentum meets the magnetic field. Hence, the neutron passes both arms of the device in a straight line in the case when there is no scattering,

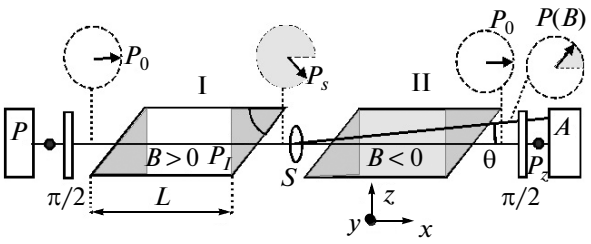

Fig. 1. Schematic diagram of the SESANS device.

and the phase of the Larmor precession accumulated in the first arm is fully compensated in the second arm, returning the neutron phase to the initial state. In the case of scattering, the neutron travels longer or shorter distances in the second arm than in the first by a length proportional to the scattering angle. As a result the difference in the phase of the Larmor precession between the scattered and unscattered neutrons is accumulated during the experiment.

At present, spin-echo small-angle neutron scattering (SESANS) is a novel, promising method for determining the characteristics of materials in real space [3–5]. The method allows to work in the region of the direct beam and does not require high-accuracy collimation. Due to the fact that the scattering angles are lower for the larger length scale of scattering irregularities, an obvious advantage of the method is the high intensity of neutrons for larger characteristic sizes of investigated objects from 10 to 20000 nm in comparison with regular small-angle scattering.

Devices using the method of neutron spin echo (SE) are classified according to the value of the inelastic scattering, which varies during the course of the experiment, on NSE devices, which examine inelastic scattering on the sample and investigate its correlation in time, and SESANS devices, which investigate elastic scattering on the sample and space correlation in the materials. Depending on the type of device, the angle θ_0 between the neutron beam and magnetic field changes. In the case of inelastic NSE the θ_0 angle is set at 90°, because a change in the neutron velocity occurs upon inelastic scattering, and the same path length for scattered and unscattered neutrons will be travelled in a different time. On the other hand, the θ_0 value is set below 90° for SESANS in order to create a path length difference for scattered and unscattered neutrons.

The objective of this work is validation of the SESANS device assembled at the VVR-M reactor at the St. Petersburg Institute of Nuclear Physics (Gatchina). We suggest a method for calibration of the measuring scale of the SESANS device using samples of colloidal crystals containing monodisperse spheres of known radius. We construct a calibration curve of the dependence of the SE distance on the field at the center of the main magnets of the device, and samples of colloidal SiO_2 particles are investigated by means of SESANS. It is shown that the SESANS device (St. Petersburg Institute of Nuclear Physics) is a reliable, sensitive instrument for measuring large particles and irregularities.

OPERATION PRINCIPLE OF THE SESANS DEVICE

The theory of the SESANS method is described in detail in a number of publications [3–7]. It is based on decoding the direction of neutron flight through the precession device via the value of the precession angle φ. The polarization after the device is determined via the precession angle φ in the form:

$$P(\varphi) = P_0 \cos\varphi. \quad (1)$$

The precession angle is determined as

$$\varphi = c\lambda BL\frac{\sin\theta_0}{\sin(\theta_0-\theta)} \cong c\lambda BL(1-\theta\cot\theta_0), \quad (2)$$

where θ is the angle between the direction of the neutron and the beam axis, B is the magnetic field in the precession device, and L is the length of the device. Two such devices with oppositely directed fields (or parallel fields and a spin-flipper between them) allow the small-angle scattering to be measured on the sample located between them. A schematic representation of this device is given in Fig. 1.

According to Eq. (2), the difference in the precession angles Δφ after the passage of the two precession devices at the angles θ_1 and θ_2, respectively, is determined as

$$\Delta\varphi = \varphi_1 - \varphi_2 = c\lambda BL\cot\theta_0(\theta_2-\theta_1) = \delta Q_z, \quad (3)$$

where

$$\delta = \frac{c\lambda^2 BL\langle\cot(\theta_0)\rangle_\alpha}{2\pi} \text{ and } Q_z = \frac{2\pi}{\lambda}(\theta_2-\theta_1). \quad (4)$$

The constant c equals $2\pi\mu_n m_n/h^2$ ($=4.63\times10^{14}$ T^{-1} m^{-2}), with μ_n and m_n neutron mass and magnetic moment, respectively. Here, Q_z is the transmitted scattering transfer of the momentum in the z direction perpendicular to the neutron beam and at the angle θ_0 to the boundaries of magnetic field. The δ value, which is complementary to Q_z, defines the length scale, where the correlation is measured and is termed the "spin-echo length." Scanning along this length can be conducted by varying λ, B, L, or θ_0.

The measured neutron-beam polarization P_m can be presented as

$$P_m I_m = P_0 I_{ns} + P_s \times I_s, \quad (5)$$

where I_m is the intensity of the propagating beam; P_0 and I_{ns} is the polarization and intensity of the unscattered part of the beam; $P_s \times I_s$ is the convolution of the scattering cross section (probability of scattering) and polarization (P_s) of the part of the beam scattered to a solid angle θ, corresponding to the transferred momentum Q:

$$P_s^* I_s = I_0 x\frac{1}{k_0^2}\int dQ_y dQ_z P_s(Q_z)\frac{d\sigma}{d\Omega}(Q). \quad (6)$$

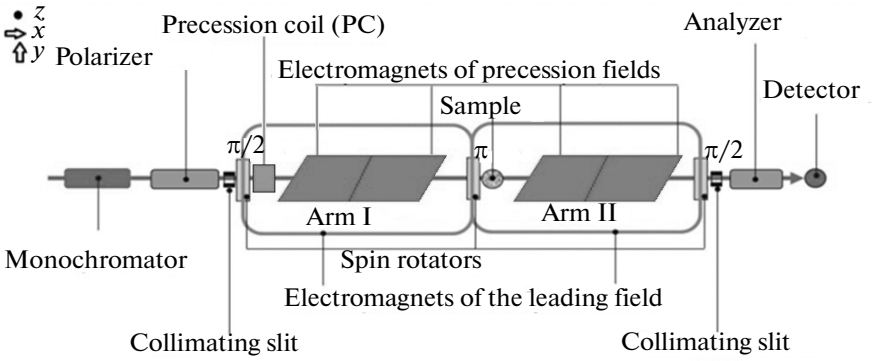

Fig. 2. Schematic representation of the SESANS device at the St. Petersburg Institute of Nuclear Physics.

Here, x is the thickness of the sample, $P_s(Q_z) = P_0\cos(Q_z\delta)$, I_0 is the intensity of the initial beam, k_0 is the value of the wave vector of the initial beam, and

$$\sigma = \frac{1}{k_0^2}\int dQ_y dQ_z P_s(Q_z)\frac{d\sigma}{d\Omega}(Q) \tag{7}$$

is the total scattering cross section. In the single scattering approximation ($\sigma x \ll 1$) [8], $I_{ns} = I_0(1-\sigma x)$ and $I_m = I_0$. Hence, the measured polarization (5) assumes the form:

$$P_m = P_0(1-\sigma x) + P_0 x\left(\frac{1}{k_0}\right)^2 \times \int dQ_y dQ_z \frac{d\sigma}{d\Omega}(Q)\cos(Q_z\delta). \tag{8}$$

In the case of a very thin sample of the thickness dx, Eq. (8) can be presented in the single scattering approximation as follows:

$$\frac{(P_m - P_0)}{P_0} \to \frac{dP}{P} = -dx\left[\sigma - \frac{1}{k_0^2}\int dQ_y dQ_z \frac{d\sigma}{d\Omega}(Q)\cos(Q_z\delta)\right], \tag{9}$$

showing that the change in polarization due to scattering is proportional to dx.

Integration of Eq. (9) along the length of the sample from 0 to l gives

$$\frac{P_m(l,\sigma)}{P_0} = \exp\{-l\sigma[1-G(\delta)]\}. \tag{10}$$

As was shown in [5], the second term in the argument of the exponential function is a projection of the spatial pair correlation function along the axis of the neutron-beam path. Hence, the so-called SESANS correlation function $G(\delta)$ can be calculated from the measured P_m value, which can be presented as follows for isotropic samples:

$$G(\delta) = \int dx\langle\rho(r)\rho(r+\delta)\rangle = \frac{1}{k_0^2}\int dQ_y dQ_z \frac{d\sigma}{d\Omega}(Q)\cos(Q_z\delta), \tag{11}$$

where $\rho(r)$ is the scattering potential at the point r.

DESCRIPTION OF THE SESANS DEVICE AT THE VVR-M REACTOR (PNPI)

Construction of the SESANS device at the St. Petersburg Institute of Nuclear Physics began in 2005. The device is located at the 14th beam of the VVR-M reactor with the wavelength $\lambda = 0.23$ nm and $\Delta\lambda/\lambda = 0.02$. The possibilities of 3D analysis and the SESANS device are combined in the instrument. The main magnets of the precession fields comprise four electromagnets with a closed steel yoke. Slanted pole extensions are installed (at an angle of 45°). Variation of the δ value is conducted by changing the magnetic-field value B at the centers of the main magnets, which is set by the current in the electromagnets. The maximum field at the center of each electromagnet is 0.1 T. Currently the device is working reliably in the mode of classic spin echo. A measurement range of the spin-echo length scale of 20–350 nm is reached.

A schematic representation of the device is given in Fig. 2. Neutrons polarized along the z axis arrive at the $\pi/2$ rotator, where the vector of the beam polarization is rotated by 90° and coincides with the y axis, followed by rotation by the precession coil (PC) around the z axis by an angle from 0 to 2π depending on its current. Next, neutrons enter non-adiabatically (through the abrupt boundary of the field) into the magnetic field of the first arm of the device directed along the z axis, where the precession of neutron spin occurs. Neutrons arrive in the second arm after passing the first arm, being turned in the flipper by 180° around the y axis. Further, the neutron beam enters the $\pi/2$ rotator,

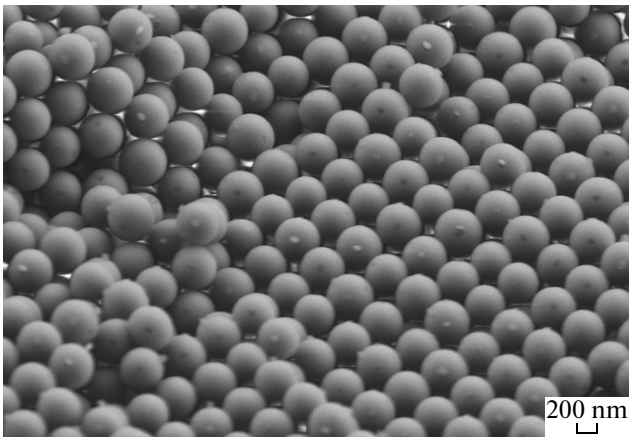

Fig. 3. SEM image of the surface of Sample-3 with a sphere diameter of $d = 485$ nm.

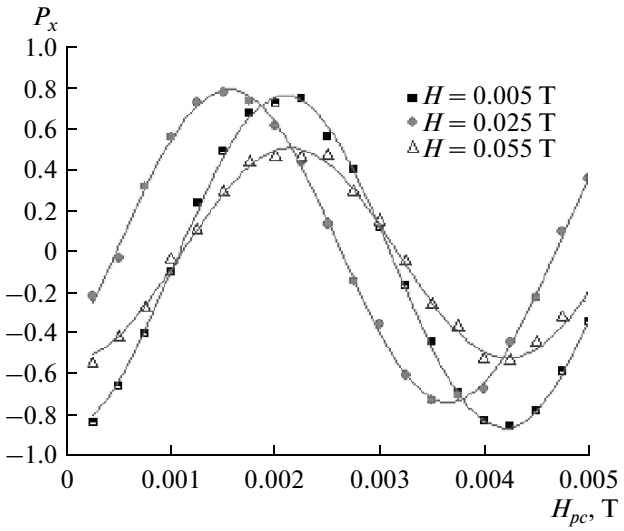

Fig. 4. Representation of one period of the spin-echo group for fixed currents in the main magnets for Sample-1.

where the beam polarization rotates again by 90°. After that, neutrons with spin polarization along the z axis are detected, while the analyzer adsorbs neutrons with spin directed against the field.

TEST (CALIBRATION) EXPERIMENT

Samples of colloidal particles consisting of ordered monodisperse SiO_2 spheres were used for device validation. The spheres form a dense three-dimensional structure and, hence, the distance between the neighboring particles is determined by the diameter of the spheres. The characteristic radius of the spheres in the samples was first determined via scanning electron microscopy (SEM) and small-angle X-ray scattering (SAXS) [9]. A SEM image of the surface of Sample 3 is presented in Fig. 3. It can be seen from the figure that the spheres are monodisperse and do not form agglomerates; their diameter is 485 nm. The results of determination of the size of the samples with both methods are presented in the table.

Three samples with different sphere sizes: Sample-1 ($R = 175 \pm 4$ nm), Sample-2 ($R = 203 \pm 4$ nm), and Sample-3 ($R = 257 \pm 5$ nm) were selected for the measurements. The measurements were conducted with the SESANS device of the St. Petersburg Institute of Nuclear Physics (Gatchina). Polarization of the neutron beam as a function of the field at the center of the precession coil for a fixed current in the main magnets of the device was measured in the experiment. The range of the field at the center of the coil was selected in such a way that one rotation period of the neutron beam in the field directed along the z axis would fit in it, that is from 0 to 5 mT with a step 0.25 mT. Typical patterns of the spin-echo signals for three different fields of the main magnets are presented in Fig. 4. The experimental points of the spin-echo signal were approximated with the $P_i\sin(B + \varphi_0)$ function. The values of the function amplitude, which correspond to the values of the polarization component of the neutron beam perpendicular to the field, were obtained from the approximation. The measurement range along the field at the center of the main magnets was $0.005 \le B_{mm} \le 0.055$ T, with a step in the field of $\Delta B_{mm} = 0.005$ T. The dependences of the amplitude of the SE signal on the field of the main magnets $P_z/P_0(B_{mm})$ were obtained from the ratio of the polarization value after scattering on the sample to the polarization of the initial beam.

Sphere radii of the investigated samples measured with SAXS and SEM methods [8]

Sample	Sample-1	Sample-2	Sample-3
R_{SAXS}, nm	175 ± 4	203 ± 4	257 ± 5
R_{SEM}, nm	165 ± 11	193 ± 12	243 ± 3

Since the field in the magnet changes significantly along the beam from the center to the edges of the magnet, and the angle between the beam and magnetic field θ_0 cannot be determined with sufficient accuracy, the $\delta(B_{mm}, \theta_0)$ parameter also cannot be determined with an accuracy sufficient for conducting precise measurements. In this context the necessity exists for calibration of the spin-echo length scale of the device according to the field measured at the centers of the main magnets B_{mm}. The δ-scale of the device was calibrated using Sample-3. The theoretical curve of the dependence of P_z/P_0 on δ was constructed for spheres with a radius of 257 nm (Fig. 5a). The dependence of the amplitude of the spin-echo signal on the spin-echo length was approximated using Eqs. (10)–(11). The

$G(\delta)$) function can be represented as a sum of the autocorrelation and pair correlation functions. The autocorrelation function provides a major contribution to $G(\delta)$ in the range of low δ and, hence, the $G_{SE}(\delta)$ equations can be used for fitting the experimental data in the case of dilute monodisperse spheres [5]:

$$G_{SE}(\delta) = \sqrt{1-\left(\frac{\delta}{2R}\right)^2}\left(1+\frac{1}{8}\left(\frac{\delta}{R}\right)^2\right) + \frac{1}{2}\left(\frac{\delta}{R}\right)^2\left(1-\left(\frac{\delta}{4R}\right)^2\right)\ln\left(\frac{\delta}{R}\Big/\left(2+\sqrt{4-\left(\frac{\delta}{R}\right)^2}\right)\right). \quad (12)$$

The experimentally obtained P_z/P_0 values for this sample were correlated with the points of the curve. The spin-echo length $\delta(P_z/P_0)$ was matched with each value of the magnetic field $H(P_z/P_0)$ (Fig. 5b). The applicability of this calibration was tested using Sample-1 and Sample-2.

The dependences of the amplitude of the spin-echo signal on the parameter δ for Sample-1 and Sample-2 are presented in Fig. 6a. Considering that the P_z/P_0 ratio depends exponentially on the correlation function $G(R)$, the decrease in P_z/P_0 with an increase in δ observed on the curves indicates a decrease in the correlation between the points of the sphere with increasing correlation length. The $G(R)$ function of the polycrystal comprises periodic decaying modulations with a period close to the distance between the centers of the closest neighbors. The modulations cannot be seen on the presented dependences because the periods of the measured samples are greater than the maximum δ value. An observed slight increase in the P_z/P_0 for larger δ in the case of Sample-1 indicates the proximity of the maximum in the range $\delta \approx D = 350$ nm.

The dependences of the amplitude of the spin-echo signal on δ for Sample-1 with different thicknesses are presented in Fig. 6b. It can be seen that the maxima and minima on the graphs are observed at the same δ values, which implies that the spheres are identical in size in the samples. The curves do not coincide, however, which is due to differences in the total scattering cross section for samples of different thicknesses.

All graphs of the dependences of the amplitude of the spin-echo signal were approximated with Eqs. (10) and (11). The values of the total scattering cross section s_t for each sample were obtained from the results of approximation. The values of the amplitude of the spin-echo signal P_z/P_0 were transformed into G_{SE}, s_t taking into consideration. The dependences $G_{SE}(\delta)$ are presented in Fig. 7. It is obvious that the $G_{SE}(\delta)$ experimental graphs for Sample-1 of different thicknesses are in good agreement within the measurement error.

The experimental values of the sphere radii were elucidated from approximations of the dependences of the autocorrelation functions for the dilute spheres: $R_{\text{Sample-1}} = 161 \pm 7$ nm; $R_{\text{Sample-2}} = 195 \pm 6$ nm; $R_{\text{Sample-3}} =$

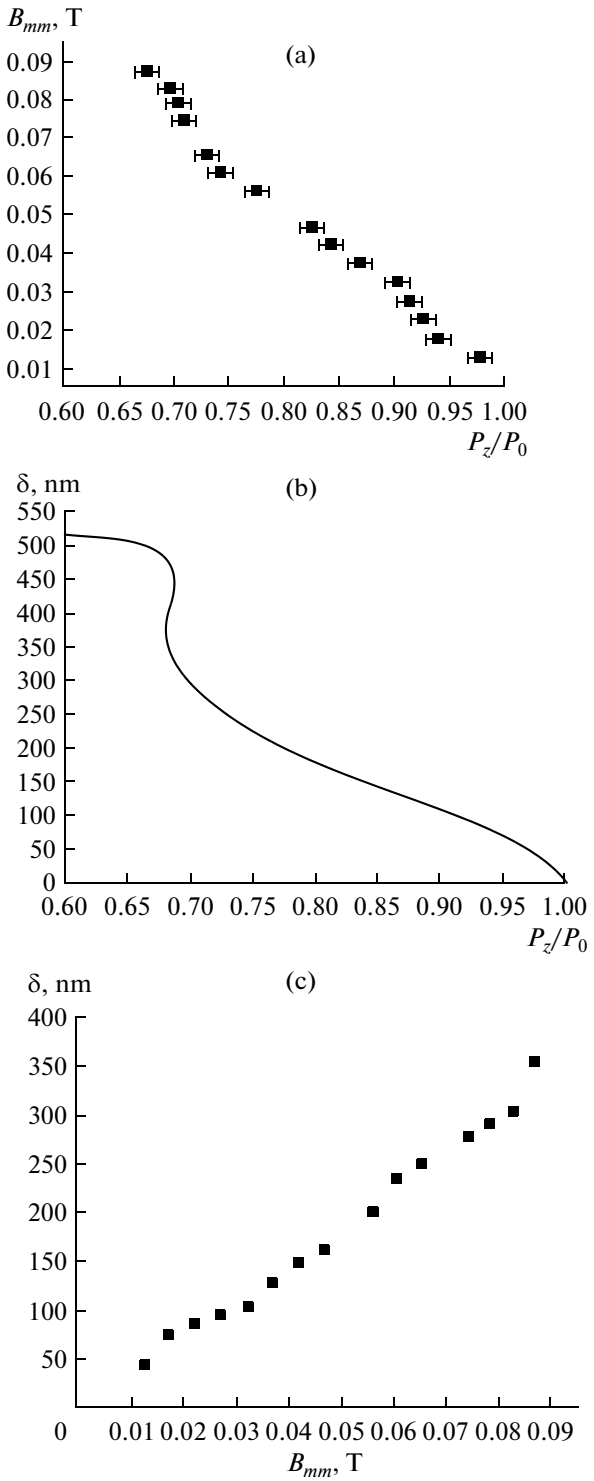

Fig. 5. Calibration of the spin-echo length scale of the device: (a) the experimentally obtained dependence of the amplitude of the spin-echo signal on the field at the center of the main magnets for Sample-3 with a sphere diameter of 257 nm; (b) the theoretical curve of the dependence of the amplitude of the spin-echo signal on the spin-echo length calculated with Eq. (12); (c) the calibration curve for the dependence of the spin-echo length on the field magnitude at the centers of the main magnets.

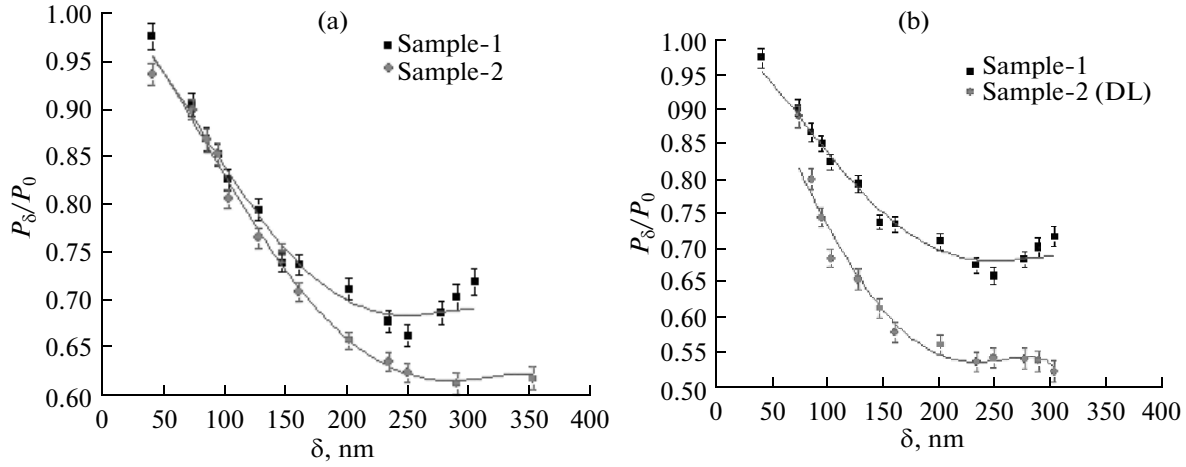

Fig. 6. Dependences of the amplitude of the spin-echo signal on the spin-echo length (a) for all samples, and (b) on the thickness of Sample-1.

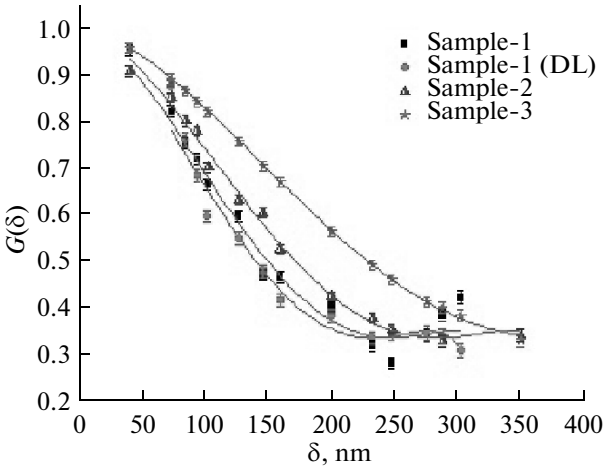

Fig. 7. Dependences of the spin-echo correlation function on the spin-echo length for all samples approximated with the autocorrelation function of the dilute monodisperse spheres.

261 ± 5 nm. The experimental R_{SE} values are in agreement with the validated values within the limits of error.

CONCLUSIONS

A method was developed for the calibration of SESANS devices, which was used for calibration of the SESANS device at the St. Petersburg Institute of Nuclear Physics. The first scattering experiments were conducted with samples of opal-like particles consisting of SiO_2 spheres validated with SEM and SAXS methods. The experimental values of the sphere radii coincided with the validated values, which suggest the high accuracy of the obtained results. It was shown that the SESANS device at the St. Petersburg Institute of Nuclear Physics was a reliable, sensitive instrument for the measurement of large structures.

ACKNOWLEDGMENTS

We are grateful to Masalov and Emel'chenko for providing the samples and to the resource center of the St. Petersburg State University for investigation of the samples via SEM.

This work was supported by the Russian Foundation for Basic Research, projects nos. 12-02-12066-ofi-m, 12-02-31242 mol-a).

REFERENCES

1. F. Mezei, Z. Phys. **255**, 146 (1972).
2. F. Mezei, *Neutron Spin Echo*, Lecture Notes in Physics, Vol. 128 (Springer, Berlin, Heidelberg, 1980), pp. 3–26.
3. M. Th. Rekveldt, J. Nucl. Insrum. Methods Phys. Res. B **114**, 366 (1996).
4. M. Th. Rekveldt, W. G. Bouwman, W. H. Kraan, et al., in *Neutron Spin Echo*, Lecture Notes in Physics, Vol. 601 (Springer, Berlin, 2002), p. 87.
5. M. Th. Rekveldt, W. G. Bouwman, W. H. Kraan, et al., in *Neutron Spin Echo*, Lecture Notes in Physics, Vol. 601 (Springer, Berlin, 2002), p. 100.
6. M. Th. Rekveldt, J. Plomp, W. G. Bouwman, et al., Rev. Sci. Instrum. **76**, 03390 (2005).
7. T. Kruglov, I. M. de Schepper, W. G. Bouwman, et al., J. Appl. Crystallogr. **36**, 117 (2003).
8. S. V. Grigoriev, W. H. Kraan, M. Th. Rekveldt, et al., J. Appl. Crystallogr. **39**, 252 (2006).
9. N. A. Grigorieva, in *Proceedings of the 46th School of Peterb. Institute of Nuclear Physics on Physics of Condensed States* (St.-Petersburg, 2012), p. 86.

Translated by L. Brovko